



## Search for $WH$ associated production using neural networks with $5.0 \text{ fb}^{-1}$ of Tevatron data

The DØ Collaboration

URL: <http://www-d0.fnal.gov>

(Dated: August 13, 2009)

A search is presented for  $WH$  production in  $p\bar{p}$  collisions at a center of mass energy of  $\sqrt{s} = 1.96 \text{ TeV}$ , combining the full Tevatron Run IIa data with most of the current Run IIb data, the total corresponding to an integrated luminosity of  $5.0 \text{ fb}^{-1}$  accumulated by the DØ experiment. Events containing one lepton, an imbalance in transverse energy and one or two tagged  $b$  jets are selected using a neural network to enhance the potential  $WH$  signal over standard model background. Good agreement between data and the background prediction is observed for the single and double  $b$ -tagged samples. We set a combined upper limit of 6.9 (5.1) for  $m_H = 115 \text{ GeV}$  at 95% confidence level on the ratio of  $\sigma(p\bar{p} \rightarrow WH) \times B(H \rightarrow b\bar{b})$  to its standard model prediction for the observed (expected) result.

*Preliminary Results for the Lepton-Photon 2009 Conference*

## I. INTRODUCTION

The most sensitive channel at the Tevatron for a low mass Higgs boson (below  $\sim 125$  GeV) is the associated production of a Higgs boson with a  $W$  boson. Several searches for  $WH$  production have been published at a center-of-mass energy of  $\sqrt{s} = 1.96$  TeV. Three of these [1–3] used subsamples ( $0.17$  fb $^{-1}$ ,  $0.44$  fb $^{-1}$ , and  $1.1$  fb $^{-1}$ ) of the data analyzed in this conference note, while two others, from the CDF collaboration, are based on  $0.32$  fb $^{-1}$  and  $0.95$  fb $^{-1}$  of integrated luminosity [4, 5].

This note presents a new search using neural networks on  $5$  fb $^{-1}$  of data. The search is based on events with one lepton ( $e$  or  $\mu$ ), an imbalance in transverse energy,  $\cancel{E}_T$ , to account for the neutrino in the decay of the  $W$  boson, and either two or three jets, with one or two of these jets being  $b$ -tagged, since  $H \rightarrow b\bar{b}$  is the dominant SM Higgs decay at low mass.

The channels are separated into events with exactly one “tight”  $b$ -tagged jet, and those with two “loose”  $b$ -tagged jets (with no overlap).

In events with two  $b$ -tagged jets, the dominant backgrounds to  $WH$  are  $Wb\bar{b}$  production,  $t\bar{t}$  and single-top quark production. In single  $b$ -tagged events, multijet events and  $W$  production in association with  $c$  and/or light jets also provide important contributions to the background.

We apply a neural network (NN) to the selected events to separate the standard model (SM) background from signal, and search for an excess at high values of the discriminant. The neural network has seven kinematic input variables.

The four  $W + 2$  jet channels ( $e$  and  $\mu$  for 1 and 2  $b$ -tags) are analyzed independently to optimize sensitivity, and then combined. In parallel, the four analogous channels in  $W + 3$  jet events are also analyzed, using the dijet invariant mass as discriminant, and also combined with the other four channels.

The data correspond to an integrated luminosity of  $5.0$  fb $^{-1}$  after requiring good data quality criteria and have been recorded between April 2002 and February 2006 (full Run IIa  $\sim 1.1$  fb $^{-1}$ ) and between June 2006 and April 2009 (part of Run IIb  $\sim 3.9$  fb $^{-1}$ ). Between Run IIa and Run IIb the DØ detector was upgraded. In particular the triggering system was improved, and a new layer of silicon sensors of the microvertex detector was installed closer to the beam pipe, providing more precise track reconstruction. The two data periods are analyzed independently and their results are subsequently combined.

## II. DATA SAMPLE

The analysis relies on the following components of the DØ detector [6]: a central-tracking system, which consists of a silicon microstrip tracker (SMT) and a central fiber tracker (CFT), both located within a 2 T superconducting solenoidal magnet; a liquid-argon/uranium calorimeter consisting of a central section (CC) covering pseudorapidity (relative to the center of the detector)  $|\eta|$  [7] up to  $\sim 1.1$ , and two end calorimeters (EC) extending coverage to  $|\eta| < 4.0$ , all housed in separate cryostats [8], with scintillators between the CC and EC cryostats providing sampling of developing showers at  $1.1 < |\eta| < 1.4$ ; a muon system that resides beyond the calorimetry, and consists of layers of tracking detectors and scintillation trigger counters before and after the 1.8 T iron toroids.

Luminosity is measured using plastic scintillator arrays located in front of the EC cryostats, at  $2.7 < |\eta| < 4.4$ . The uncertainty on the measured luminosity is 6.1% [9]. We reject data periods in which the tracking (CFT and SMT), calorimeter or muon information may have been compromised.

The trigger and data acquisition systems are designed to accommodate the high instantaneous luminosities of Run II. The events used in this analysis are triggered in the electron channel by a logical OR of several triggers requiring an electromagnetic (EM) object and one jet. Trigger efficiencies are taken into account in the simulation through event reweighting based on an efficiency derived from data, and parametrized as a function of lepton azimuthal angle  $\phi$  and  $\eta$ , and jet  $p_T$ . This efficiency is on average  $\sim 90\%$  for events passing acceptance requirements.

In the muon analysis we accept events from any trigger, since we expect close to 100% of events to be triggered by our redundant triggering system (single muons, muon+jets, topological triggers). This is verified using a combination of single-muon triggers for which a full analysis is completed. The efficiency of the single-muon trigger combination is measured on dimuon  $Z$  events with an uncertainty of 3%, and is  $\sim 70\%$  for events passing the selection cuts. This efficiency is consistent within  $\pm 3\%$  for the high statistics (pre  $b$ -tagged) channels, and within  $\pm 10\%$  for the low statistics ( $b$ -tagged) samples. An increase in statistics of 47% is observed when accepting events from any trigger in data, consistent with a trigger efficiency of 100% for the selected events. The shape of all distributions remains unchanged within systematic uncertainty originating mainly from the uncertainty in jet energy scale. We thus use all triggers for the final analysis, after attributing an additional 5% uncertainty on trigger systematics in this channel.

### III. SIMULATED DATASETS

Simulation of background and signal processes relies on the CTEQ6L1 [10] leading-order parton distribution functions and uses the following event generators. The PYTHIA [11] Monte Carlo (MC) generator has been used for the following processes:

- Exclusive diboson production and inclusive decay of  $WW$ ,  $WZ$  and  $WZ$ .
- Exclusive  $WH \rightarrow \ell\nu b\bar{b}$  production ( $\ell = e, \mu, \text{ or } \tau$ )
- Exclusive  $ZH \rightarrow \ell\ell b\bar{b}$  production ( $\ell = e, \mu, \text{ or } \tau$ )

The following processes are simulated using other generators:

- $W$ + jets and  $Z$ + jets events are generated with ALPGEN [12] (interfaced to PYTHIA for parton showering and hadronization) because ALPGEN yields a better description of processes with high jet multiplicity. ALPGEN samples are produced using the MLM parton-jet matching prescription [12] and are generated in bins of light parton multiplicity.  $W(Z)$ + jets samples contain  $W(Z)jj$  and  $W(Z)cj$  processes, while  $W(Z)b\bar{b}$  and  $W(Z)c\bar{c}$  are generated separately, also with ALPGEN+ PYTHIA.
- $t\bar{t}$  (lepton+jet and dilepton channels) production is generated with ALPGEN+ PYTHIA.
- Single-top events ( $s$ -channel  $tb$  and  $t$ -channel  $tbq$ ) are generated using COMPHEP [13], and PYTHIA for parton evolution and hadronization.

All generated events are processed through the DØ detector simulation (based on GEANT [14]) and the same reconstruction software as for data. Simulated events are reweighted for differences in trigger efficiencies of MC simulations relative to data (scale factors), which depend on the specific data samples. These scale factors can be constants or can depend on event kinematics, all of which is taken into account in the analysis.

The simulated background processes are normalized to the SM predictions for their cross sections, except for  $W$ + jets samples which are normalized to data in the pre-tagged sample, where the contamination from signal is expected to be negligible. The data/MC normalization factor is found to be  $\sim 1.0 \pm 0.1$  from comparisons of data with Next-to-Leading-Order (NLO) predictions for  $W$ + jets based on the MCFM program [15] (the normalization factor is obtained after subtracting all other expected background processes from data). For the  $Wb\bar{b}$  and  $Wc\bar{c}$  samples we introduced an additional multiplicative factor,  $s_{hf}$ , of  $1.05 \pm 0.2$ , relative to the NLO prediction, by adjusting the total number of background events to data in the  $W + 2$  jet sample with 0  $b$ -tagged jets. Overall, the experimentally determined value is consistent with the ratio of the K-factors for  $Wb\bar{b}$  and  $W$ + light jets obtained from MCFM. The same factors are used for the corresponding  $Z$ + jet processes.

### IV. EVENT SELECTION

The analysis is based on the selection of events with only one electron with  $p_T > 15$  GeV and  $|\eta| < 1.1$  or  $1.5 < |\eta| < 2.5$ , or with only a single muon with  $p_T > 15$  GeV and  $|\eta| < 2.0$ . Events are also required to have an imbalance in transverse energy of  $\cancel{E}_T > 20$  GeV, either two or three jets with  $p_T > 20$  GeV (following jet energy calibration) and  $|\eta| < 2.5$ , and the sum of the  $p_T$  of the jets,  $H_T$ , to exceed 60 GeV (80 GeV for the 3-jet sample).

Events with additional electrons (muons), isolated from jets and with  $p_T > 20$  GeV ( $> 15$  GeV) are rejected to decrease dilepton background from  $Z$  and  $t\bar{t}$  events. Only events with a primary  $z$ -vertex within  $\pm 40$  cm of the nominal longitudinal interaction point, and at least three emanating charged tracks are selected for further analysis.

#### A. Lepton reconstruction and identification

The leptons used in the analysis are identified in two steps.

(i) The lepton candidates must first pass the “loose” identification criteria, which for the electron requires the fraction of energy deposited in the EM calorimeter to be  $> 0.95$ , the ratio of the energy within an annular ring defined by external and internal radii of  $R = 0.4$  and  $0.2$  around the electron candidate’s direction, divided by the total energy, to be  $< 0.10$ ; the reconstructed electron track must pass isolation criteria, EM shower-shape requirements, and have a spatially matched track to the EM shower with probability  $> 0.001$ . For the loose muon, we require hits in each layer of the muon system, no scintillator hits timed cuts to veto cosmic rays, a match of the muon track and a central

track, and isolation from jets to reject muons from semi-leptonic decay of hadrons ( $\Delta R < 0.5$ ) [7].

(ii) The loose leptons then undergo a final “tight” selection: tight electrons have to satisfy more rigid isolation criteria, incorporate a larger EM fraction and satisfy a likelihood test developed on well-controlled data samples that is based on eight quantities sensitive to the EM nature of the particles [16]; tight muons must satisfy stricter isolation criteria requiring low calorimeter and tracking activity around the muon candidate. Inefficiencies introduced by lepton identification and isolation criteria are determined from dielectron and dimuon samples. The final selection uses only tight leptons with loose leptons used to determine instrumental and semi-leptonic backgrounds.

## B. Instrumental and semi-leptonic background

Instrumental backgrounds and those from semi-leptonic decays of hadrons, referred to jointly as multijet background below, are estimated from data. The instrumental background is important for the electron channel, where a jet with high EM fraction can pass the electron identification criteria, or a photon can be misidentified as an electron. In the muon channel, the multijet background is due to events in which a muon from a semi-leptonic heavy quark decay is misidentified as isolated.

To estimate the number of events containing a jet passing final electron identification criteria, we determine the probability,  $p_{tight}^{loose}$ , for a loose electron candidate originating from a jet to also pass the tight identification criteria. This is done on events that pass the preselection requirements, i.e. containing one loose lepton and two jets, but with low  $\cancel{E}_T$  (5 – 15 GeV), in which one of the jets has an EM fraction smaller than 0.7, is in the central calorimeter ( $|\eta| < 1.1$ ) and far from boundaries of calorimeter modules. The probability  $p_{tight}^{loose}$  is obtained by dividing the number of events with at least one tight electron candidate by the total number of events in the sample. This probability is determined as a function of the  $p_T$  of the electron candidate. We proceed similarly in the muon channel to determine the semi-leptonic background. We use the same selection criteria, but require a loose muon to be back-to-back in  $\phi$  with one of the jets.

The multijet background is then estimated for every differential distribution: this  $p_T$ -dependent probability is used in the “matrix method” that we apply to our final sample and to the loose sample. Once  $p_{tight}^{loose}$  and the efficiency to misidentify a true loose lepton as tight are known [16], this method offers a way to extract the multijet background directly from data. The  $p_T$  distribution of the lepton in the  $W + 2$  jet sample is shown in Fig.1a and is compared to the expectation. After adding the multijet background and other SM backgrounds detailed in the previous sections, the shape of the distribution is well reproduced by the ALPGEN simulation of the  $W +$  jets processes.

## C. $\cancel{E}_T$ and jet properties

To select  $W$  decays we require  $\cancel{E}_T > 20$  GeV. where  $\cancel{E}_T$  is calculated from the calorimeter cells except for unclustered energy in cells in the coarse-hadronic layers, and is corrected for the presence of any muons. All energy corrections to electrons or to jets are propagated into  $\cancel{E}_T$ .

The transverse mass  $m_T = \sqrt{2p_T^\ell p_T^\nu (1 - \cos(\phi_\ell - \phi_\nu))}$  of the  $W$  boson can be reconstructed from the kinematics of the charged lepton and the neutrino ( $\nu$ ), in which the neutrino transverse momentum is approximated by  $\cancel{E}_T$ . Its distribution is shown in Fig. 1b and the distributions of  $H_T$  and  $\cancel{E}_T$  are shown in Figs. 1c and 1d.

Jets are reconstructed using a midpoint cone algorithm [18] with a radius of  $\Delta R_y = \sqrt{(\Delta y)^2 + (\Delta \phi)^2} = 0.5$ , where  $y$  is the jet rapidity. Identification requirements ensure that the distribution in jet energy for all layers of the calorimeter is reasonable and that jets are not caused by spurious depositions of energy. The difference in efficiency for jet identification and jet resolution between data and simulation is taken into account in the overall scale factor for jet reconstruction efficiency. Comparison of ALPGEN with other generators and with data show discrepancies in distributions of jet pseudorapidity and dijet angular separations [19]. The data are therefore used to correct the ALPGEN  $W+$  jets and  $Z+$  jets MC samples by reweighting the simulated  $\eta$  of the leading and second leading jet and  $\Delta R$  between the two leading jets in the  $W/Z+$  jets samples using polynomial functions to provide agreement of the total background with the high statistics pre-tagged data sample. Additionally, a reweighting related to the ALPGEN MLM parton-jet matching algorithm, parameterized in dijet invariant mass, is applied to the  $W/Z+$  light jets MC samples.

We have studied kinematic distributions as for example the  $p_T$  distributions of the leading jet and next to leading jet in  $W + 2$  jet events which are shown in Figs. 2a and b, the distribution of  $\Delta R$  between the two jets in the  $W + 2$  jet events, shown in Fig. 2c, and the dijet invariant mass, shown in Fig. 2d. The shapes of the jet distributions are well described over the complete kinematic range.

	$W + 2$ jets	$W + 2$ jets (1 $b$ -tag)	$W + 2$ jets (2 $b$ -tag)	$W + 3$ jets	$W + 3$ jets (1 $b$ -tag)	$W + 3$ jets (2 $b$ -tag)
$WH, ZH$	$24 \pm 4$	$9.9 \pm 1.0$	$6.5 \pm 0.6$	$5 \pm 1$	$2.1 \pm 0.2$	$0.8 \pm 0.1$
$WW, WZ, ZZ$	$2208 \pm 371$	$146.1 \pm 12.5$	$22.1 \pm 1.9$	$430 \pm 72$	$29.5 \pm 2.6$	$2.3 \pm 0.2$
$W/Z + b\bar{b}$	$2544 \pm 508$	$1030.6 \pm 186.3$	$292.6 \pm 53.2$	$748 \pm 149$	$230.2 \pm 41.6$	$39.1 \pm 7.1$
$t\bar{t}$	$1114 \pm 187$	$447.2 \pm 50.4$	$201.1 \pm 22.9$	$1551 \pm 260$	$632.0 \pm 71.3$	$181.6 \pm 20.6$
Single top	$463 \pm 77$	$198.8 \pm 21.0$	$55.4 \pm 5.9$	$128 \pm 21$	$52.1 \pm 5.5$	$12.4 \pm 1.3$
Multijet	$10707 \pm 1884$	$575.9 \pm 119.8$	$47.5 \pm 9.9$	$3420 \pm 602$	$183.1 \pm 38.1$	$14.0 \pm 2.9$
$W/Z +$ jets	$68325 \pm 8745$	$1766.0 \pm 224.6$	$101.0 \pm 18.6$	$13204 \pm 1690$	$327.4 \pm 41.0$	$17.1 \pm 3.2$
Total expectation	84142 *	$4174 \pm 440$	$726 \pm 88$	18149 *	$1456 \pm 144$	$277 \pm 28$
Observed Events	84142	4162	707	18149	1480	305

\*: Normalized to the observed number of events in data

TABLE I: Summary of contributions to  $W + 2$  and  $W + 3$  jet final states. Observed events in data are compared to the number expected before tagging of events with one tight  $b$ -tagged jet, and 2 loose  $b$ -tagged jets. The expected values are based on simulation of  $WH$  and  $ZH$  (with  $m_H = 115$  GeV), dibosons ( $WW, WZ, ZZ$ ),  $Wb\bar{b}$  production, top production ( $t\bar{t}$  and single-top), multijet background and “ $W +$  jet” production, which contains light partons and  $c$  quarks. All the  $Z$  processes are simulated and included in the corresponding  $W$  categories. The processes  $W(Z)b\bar{b}$  and  $W(Z) +$  light and/or  $c$  jets are counted separately. The uncertainties given include statistical and systematic contributions.

## V. RESULTS WITH $b$ -TAGGING

Efficient identification of  $b$ -jets is central to our search for  $WH$  production. The  $D\emptyset$  neural network  $b$ -tagging algorithm [17] for identifying heavy flavored jets is based on the combination of seven variables sensitive to the presence of tracks or secondary vertices displaced significantly from the primary vertex. All tagging efficiencies are determined both from data and simulated events.

We start with a “loose” NN operating point that corresponds to a misidentification of  $\sim 1.5\%$  of “light” partons ( $u, d, s, g$ ) mistakenly tagged as heavy-flavored jets by the tagger for jet  $p_T$  of  $\sim 50$  GeV. If two jets are tagged, the event is selected as double-tagged. Otherwise, the operating point is tightened to a value corresponding to a mistag rate of about 0.5%, and the event is selected as an exclusive “tight” single  $b$ -tag, or simply called a single  $b$ -tag what follows. We are then left with two orthogonal samples, one “loose” double-tag (DT) and one “tight” single-tag (ST). This simplifies the combination of results of the separate Higgs searches in the two samples, which is done to improve sensitivity to a potential signal.

The efficiencies for identifying a jet containing a  $b$  hadron for the loose and tight operating points are  $59 \pm 1\%$  and  $48 \pm 1\%$ , respectively, for a jet  $p_T$  of 50 GeV. The efficiency is determined for taggable jets, i.e., jets with at least 2 good quality tracks and a several SMT hits. Simulated events are corrected to have the same fraction of jets satisfying the taggability and  $b$ -tagging requirements as found in data. The systematic uncertainties on the scale factors are 4-7% for heavy flavor jets ( $b, c$ ) and 10% when mistagging light jets.

The distributions in  $p_T$  for the first and second jet and of  $\Delta R$  and the dijet mass for the  $W + 2$  jet sample, in which only one jet is  $b$ -tagged, are shown in Figs. 3a–d. The observed agreement indicates that the simulation, which includes the different SM processes, describes the data very well. The analogous distributions are shown in Figs. 4a–d for the  $W + 2$  jet sample with two  $b$ -tagged jets.

The number of observed events are well described by the Monte Carlo simulation, as already shown in Table I.

## VI. NEURAL NETWORK SELECTION

To optimize the sensitivity of the search in  $W + 2$  jet events, differences between the kinematic properties of the objects in the event (lepton, jets and  $\cancel{E}_T$ ) are exploited using a neural network trained to separate Higgs signal from background. The neural network uses the following seven kinematic variables as inputs:  $p_T$ (leading jet),  $p_T$ (second leading jet),  $\Delta R$ (jets),  $\Delta\phi$ (jets),  $p_T$ (dijet system), dijet invariant mass and  $p_T$ ( $\ell - \cancel{E}_T$  system). Two separate neural networks are trained for the single tag (ST) and the double tag (DT) sample using simulated samples of  $WH$  and  $Wb\bar{b}$  events as signal and background. Separate networks are trained and used for the different Higgs masses considered in the analysis (100-150 GeV).

The most sensitive discriminant is the dijet invariant mass (shown in Figs. 5 and 6 for the different 1 and 2  $b$ -tag samples) and is therefore used as the discriminant for the  $W + 3$  jet sample. Distributions of the neural network output trained on the  $m_H = 115$  GeV sample, after all selections, are shown in Figs. 7a–d for the pre-tag and exclusive single-tag and double-tag samples. They are well described by the simulation. In Figs. 8a–d, the same distributions

are shown on a semi-logarithmic scale, and the contribution from  $WH$  indeed peaks at high values of neural network output, as opposed to background. The gain in sensitivity using this neural network approach compared to using only the dijet mass as a discriminant (measured in terms of the expected limit on the  $WH$  cross section) is of the order of 15%, depending on the Higgs mass, and is equivalent to a gain of about 20% in integrated luminosity.

## VII. SYSTEMATIC UNCERTAINTIES

The experimental systematic uncertainties due to differences in efficiencies between data and MC or to the propagation of other systematic uncertainties (trigger, energy calibration, resolution), which affect the signal and SM backgrounds (except multijet background) are summarized below. We assume that some of these systematics only affect the normalization of the signal or backgrounds, while others also affect the differential distribution of the dijet invariant mass or neural network discriminant used to derive cross section limits.

- 3-5% uncertainty on trigger efficiency derived from data, 5-6% uncertainty on lepton identification and reconstruction efficiency.
- 3% for jet taggability, 2.5-3% for  $b$ -tagging efficiency, per heavy quark jet. For the light quark jets the uncertainty is 10%; this translates into an uncertainty on the total background of the exclusive single-tag sample of 6% (negligible for double-tag).
- 5% uncertainty on acceptance for jet identification, jet energy calibration and resolution uncertainty.
- The systematic uncertainty of the ALPGEN reweighting is estimated by comparing the nominal version to a version in which the reweighting function increased or decreased by 1 standard deviation. The variations from  $\eta$  reweighting of leading and second leading jets, as well as the reweighting of  $\Delta R$  between the two leading jets, are at most of the order of 2%. The MLM parton matching reweighting applied to  $W/Z$ +light jets and the systematics associated with the choice of the renormalization, factorization and  $\alpha_S$  scales in ALPGEN are also of the order of 2%.

The systematics on the jet energy calibration, jet resolution and reweighting of the MC samples generated with ALPGEN affect the differential distribution of the final discriminant.

Overall, the experimental systematic uncertainty on the acceptance varies between 16 - 30%, depending on the process and the channel ( $\sim 15\%$  for  $WH$  in the DT channel). The uncertainty on the cross sections for background processes is 10% (12%) for  $t\bar{t}$  (single-top) production [20, 21], and 6% for diboson production. The uncertainty on  $W$  + heavy-flavor production is 20%.

## VIII. LIMIT ON $WH$ CROSS SECTION

The expected contribution from  $b\bar{b}$  decay of a SM Higgs boson of 115 GeV produced in association with a  $W$  boson is shown in Figs. 5a and b for the ST  $W+2$  and  $W+3$  jet channels, and in Figs. 5c and d for the DT  $W+2$  and  $W+3$  jet channels, respectively. The same distributions are also shown on a semi-log-scale in Figs. 6a-d.

As no excess is observed relative to expectation from SM background, we proceed to set limits using the neural network output on the  $W+2$  jet channels and the dijet mass for  $W+3$  jet events. Each channel is analyzed independently with limits derived from the sixteen individual analyses ( $e, \mu, ST, DT$ ) using the  $W+2/3$  jet events in the two data taking periods (Run IIa and b), and then combined.

Limits are calculated at 95% confidence level (C.L.) using the modified Frequentist  $CL_s$  approach with a Poisson log-likelihood ratio test statistics [22]. The impact of systematic uncertainties is taken into account, with all correlations maintained among channels and between signal and background. The expected distributions for background are evaluated by minimizing a profile likelihood function, that takes account of the shape and rate of the distributions observed in sideband regions.

The log-likelihood ratio (LLR) distributions for the  $WH \rightarrow \ell\nu b\bar{b}$ , (i.e. after combining the sixteen individual channels) is shown in Fig. 9a. Included in the figure are the LLR values for the signal + background hypothesis ( $LLR_{s+b}$ ), background-only hypothesis ( $LLR_b$ ), and the observed data ( $LLR_{obs}$ ). The shaded bands represent the 1 and 2 standard deviation departures for  $LLR_b$ . The limit on the cross section obtained for  $\sigma(p\bar{p} \rightarrow WH) \times B(H \rightarrow b\bar{b})$  is a factor of 6.9 larger than the SM expectation, at 95% C.L. for a Higgs boson mass of 115 GeV. The corresponding expected upper limit normalized to the SM cross section is 5.1. The same study is performed for ten other Higgs mass points between 100 and 150 GeV. The corresponding observed and expected 95% C.L. limits/SM expectation are given in Table II and in Fig. 9b.

$m_H$ (GeV)	expected 95% C.L. Limit/SM	observed 95% C.L. Limit/SM
	expected	observed
100	3.5	5.8
105	4.0	5.9
110	4.3	6.5
115	5.1	6.9
120	6.2	8.6
125	7.7	10.0
130	9.4	10.7
135	12.3	13.5
140	17.3	16.3
145	25.9	26.4
150	41.0	40.7

TABLE II: The 95% C.L. upper limits expected and observed on  $\sigma(p\bar{p} \rightarrow WH) \times B(H \rightarrow b\bar{b})$  divided by the corresponding SM expectation, as a function of the Higgs mass.

The improvement in sensitivity obtained with the current analysis, which combines extended acceptance and luminosity, especially in the region of best sensitivity to low Higgs masses, i.e., 115–135 GeV, with an expected limit on the yield to the SM WH cross section of 5.1 for  $m_H = 115$  GeV.

## IX. SUMMARY

The  $\ell + \cancel{E}_T + 2$  or 3 jets final states have been analyzed in a search for  $WH$  production in  $5.0 \text{ fb}^{-1}$  of data collected between April 2002 and April 2009.

Within statistical and systematic errors, the production rate of the single and double  $b$ -tagged events is in agreement with the expected SM cross sections, both for  $W + 2$  and  $W + 3$  jet events.

To search for a low mass Higgs boson, we have combined all channels ( $e, \mu, \text{ST}$  and  $\text{DT}$ ) and derived limits based on distributions of neural network discriminants in  $W + 2$  jet events, and from the dijet mass in the  $W + 3$  jet events, using the  $CL_S$  method. We set upper cross section limits on  $\sigma(p\bar{p} \rightarrow WH) \times B(H \rightarrow b\bar{b})$  divided by the SM expectation between 6 and 11 at 95% C.L. (4 to 9 for the corresponding expected limits) for Higgs masses between 100 and 130 GeV. For  $m_H = 115$  GeV, the observed (expected) 95% C.L. limit/SM is 6.9 (5.1).

## Acknowledgments

We thank the staff at Fermilab and collaborating institutions, and acknowledge support from the Department of Energy and National Science Foundation (USA), Commissariat à l’Energie Atomique and CNRS/Institut National de Physique Nucléaire et de Physique des Particules (France), Ministry for Science and Technology and Ministry for Atomic Energy (Russia), CAPES, CNPq and FAPERJ (Brazil), Departments of Atomic Energy and Science and Education (India), Colciencias (Colombia), CONACyT (Mexico), Ministry of Education and KOSEF (Korea), CONICET and UBACyT (Argentina), The Foundation for Fundamental Research on Matter (The Netherlands), PPARC (United Kingdom), Ministry of Education (Czech Republic), Natural Sciences and Engineering Research Council and West-Grid Project (Canada), BMBF (Germany), A.P. Sloan Foundation, Civilian Research and Development Foundation, Research Corporation, Texas Advanced Research Program, and the Alexander von Humboldt Foundation.

- 
- [1] D0 Collaboration, V.M. Abazov *et al.*, Phys. Rev. Lett. 94, 091802 (2005).
  - [2] D0 Collaboration, V.M. Abazov *et al.*, Phys. Lett. B 663, 26 (2008).
  - [3] D0 Collaboration, V.M. Abazov *et al.*, Phys. Rev. Lett. 102, 051803 (2009).
  - [4] CDF Collaboration, D. Acosta *et al.*, Phys. Rev. Lett. 94, 091802 (2005).
  - [5] CDF Collaboration, T. Aaltonen *et al.*, Phys. Rev. Lett. 100, 041801 (2008).
  - [6] DØ Collaboration, V. Abazov *et al.*, Nucl. Instrum. Meth., Res. A 565, 463 (2006).

- [7] Pseudorapidity  $\eta = -\ln \left[ \tan \frac{\theta}{2} \right]$ , where  $\theta$  is the polar angle as measured from the beam axis;  $\phi$  is the azimuthal angle. The  $\eta - \phi$  separation between two objects is  $\Delta R = \sqrt{(\Delta\eta)^2 + (\Delta\phi)^2}$ .
- [8] S. Abachi, *et al.*, Nucl. Instrum. Methods Phys. Res. A 338, 185 (1994).
- [9] T. Andeen, *et al.*, FERMILAB-TM-2365, April 2007
- [10] H. L. Lai *et al.*, Phys.Rev. D55 (1997) 1280, <http://hep.pa.msu.edu/people/wkt/cteq6/cteq6pdf.html>  
J. Pumplin *et al.*, JHEP07(2002)012, [arXiv:hep-ph/0201195v3](https://arxiv.org/abs/hep-ph/0201195).
- [11] T. Sjostrand, P. Eden, C. Friberg, L. Lonnblad, G. Miu, S. Mrenna and E. Norrbin, Comput. Phys. Commun. 135, (2001) 238, versions 6.319, 6.323 and 6.409.
- [12] M. Mangano *et al.*: ALPGEN hep-ph/0206293, JHEP07 (2003) 001, version 2.05, <http://mlm.web.cern.ch/mlm/alpgen>
- [13] A. Pukhov *et al.*, COMPHEP, hep-ph/9908288 (1999)
- [14] R. Brun and F. Carminati, CERN Program library Long Writeup, Report W5013 (1993).
- [15] J. Campbell and K. Ellis, MCFM, <http://mcfm.fnal.gov/>
- [16] DØ Collaboration, V. Abazov *et al.*, Phys. Rev. D 76, 092007 (2007)
- [17] T. Scanlon, FERMILAB-THESIS-2006-43 (2006)
- [18] G. Blazey *et al.*, in *Proceedings of the workshop "QCD and Weak Boson Physics in Run II"* edited by U. Baur, R.K. Ellis, and D. Zeppenfeld, Batavia (2000), p. 47. [arXiv:hep-ex/0005012](https://arxiv.org/abs/hep-ex/0005012) (2000).
- [19] J. Alwall *et al.*, Eur. Phys. C 53, 473 (2008).
- [20] N. Kidonakis *et al.*, Phys. Rev. D 78, 074005 (2008)
- [21] N. Kidonakis, Phys. Rev. D 74, 114012 (2006)
- [22] W. Fisher, FERMILAB-TM-2386-E (2007)

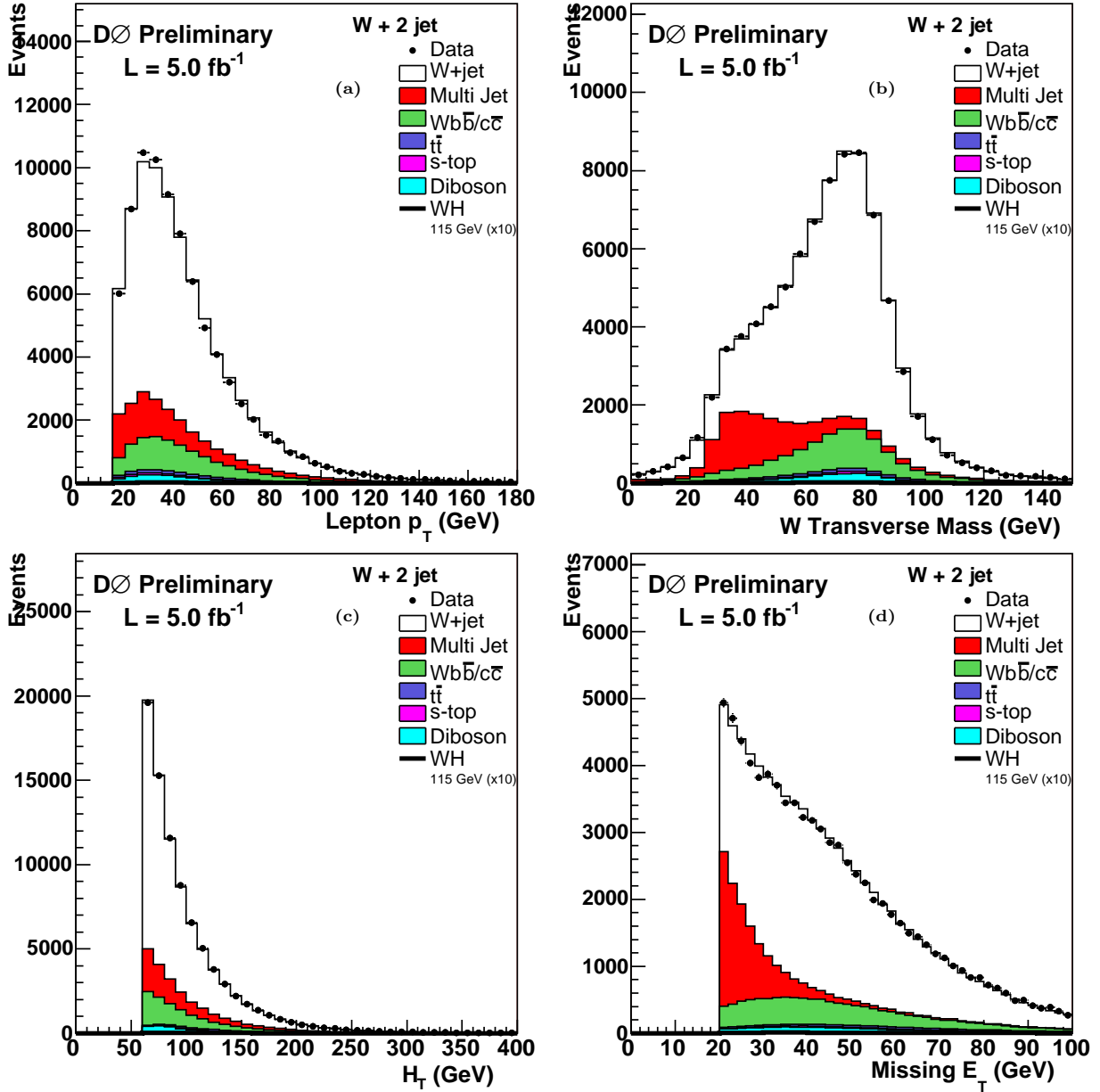


FIG. 1: Distribution in the  $W + 2 \text{ jet}$  sample of (a) the lepton momentum, (b) the transverse  $W$  mass, (c) the  $H_T$  variable and (d) the missing transverse energy compared to the simulated expectation. The simulation is normalized to the integrated luminosity of the data sample using the expected cross sections (absolute normalization) except for the  $W + \text{jets}$  sample which is normalized to the data in the untagged sample, taking into account all the other backgrounds.

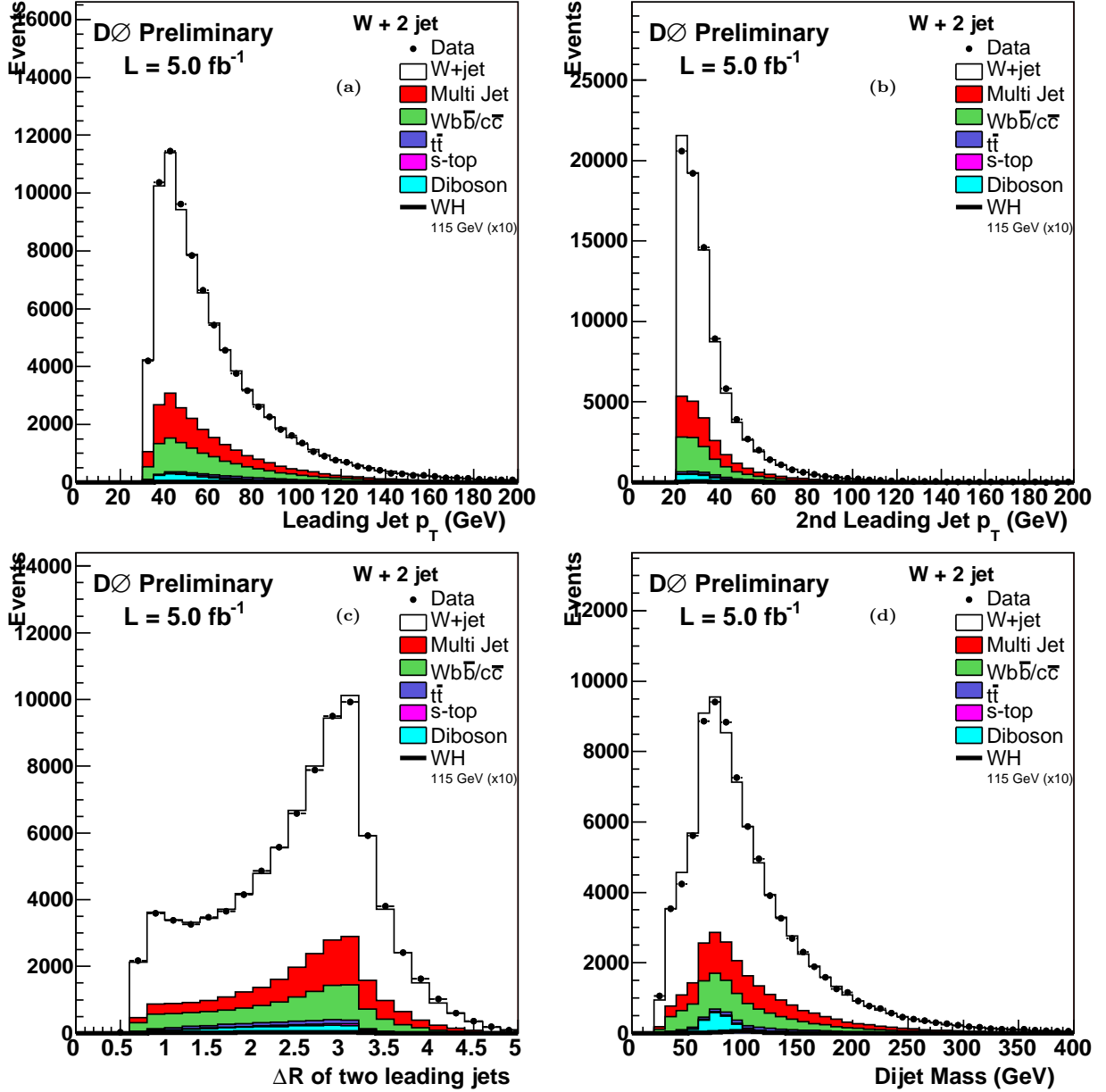


FIG. 2: Distribution in the  $W + 2$  jet sample of (a) the  $p_T$  of the leading and (b) the next to leading jet, (c) the distance in the  $\eta - \phi$  plane between the two jets and (d) the dijet mass compared with the simulated expectation. The simulation is normalized to the integrated luminosity of the data sample using the expected cross sections except for the  $W +$  jets sample which is normalized to the data in the untagged sample, taking into account all the other backgrounds.

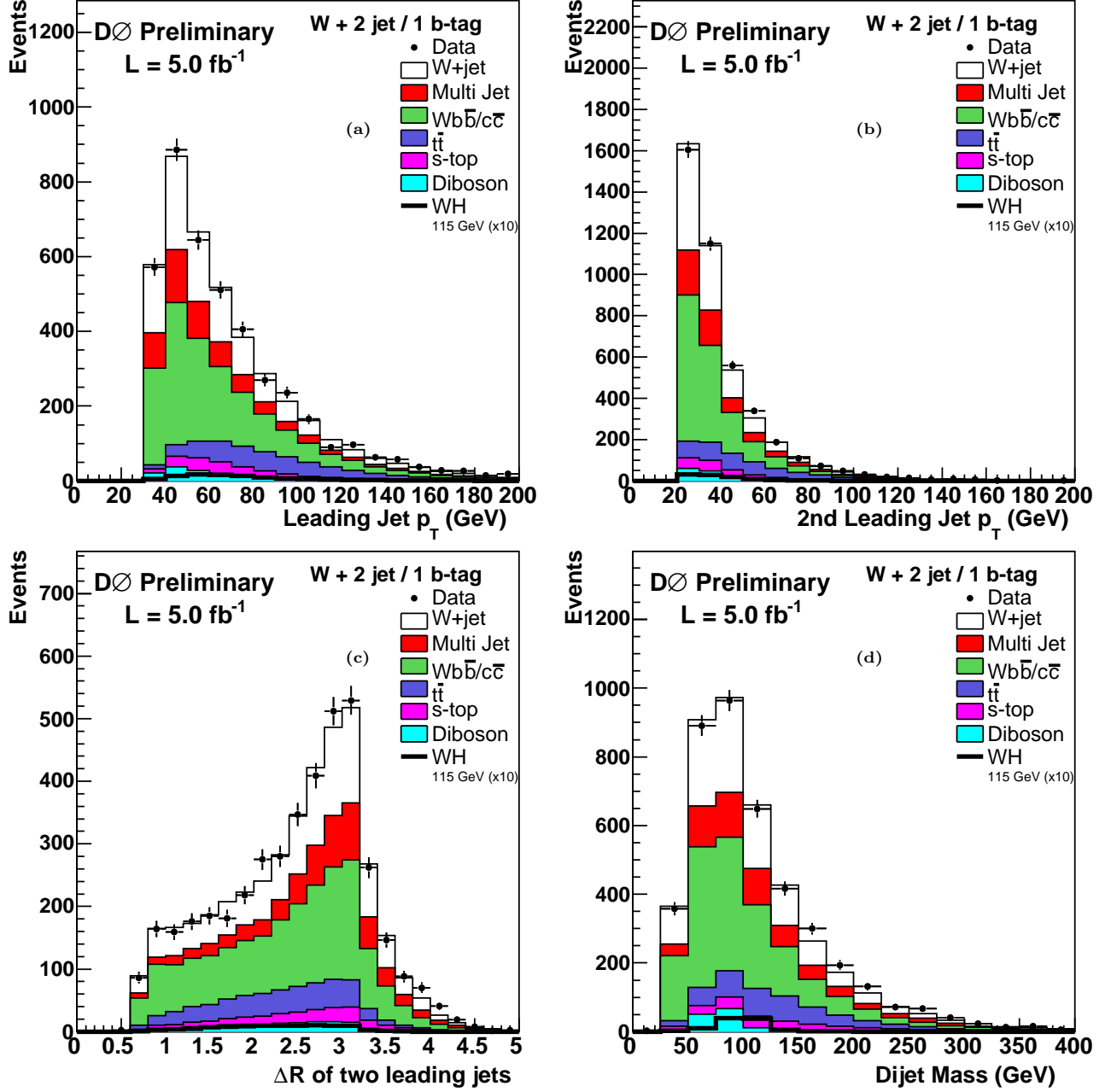


FIG. 3: Distribution in the  $W + 2$  jet sample with one  $b$ -tagged jet of (a) the  $p_T$  of the leading and (b) the next to leading jet, (c) the distance in the  $\eta - \phi$  plane between the two jets and (d) the dijet mass between the two jets compared with the simulated expectation. The simulation is normalized to the integrated luminosity of the data sample using the expected cross sections except for the  $W+$  jets sample which is normalized to the data in the untagged sample, taking into account all the other backgrounds. Also shown is the contribution expected for SM  $WH$  production with  $m_H = 115$  GeV, multiplied by a factor 10.

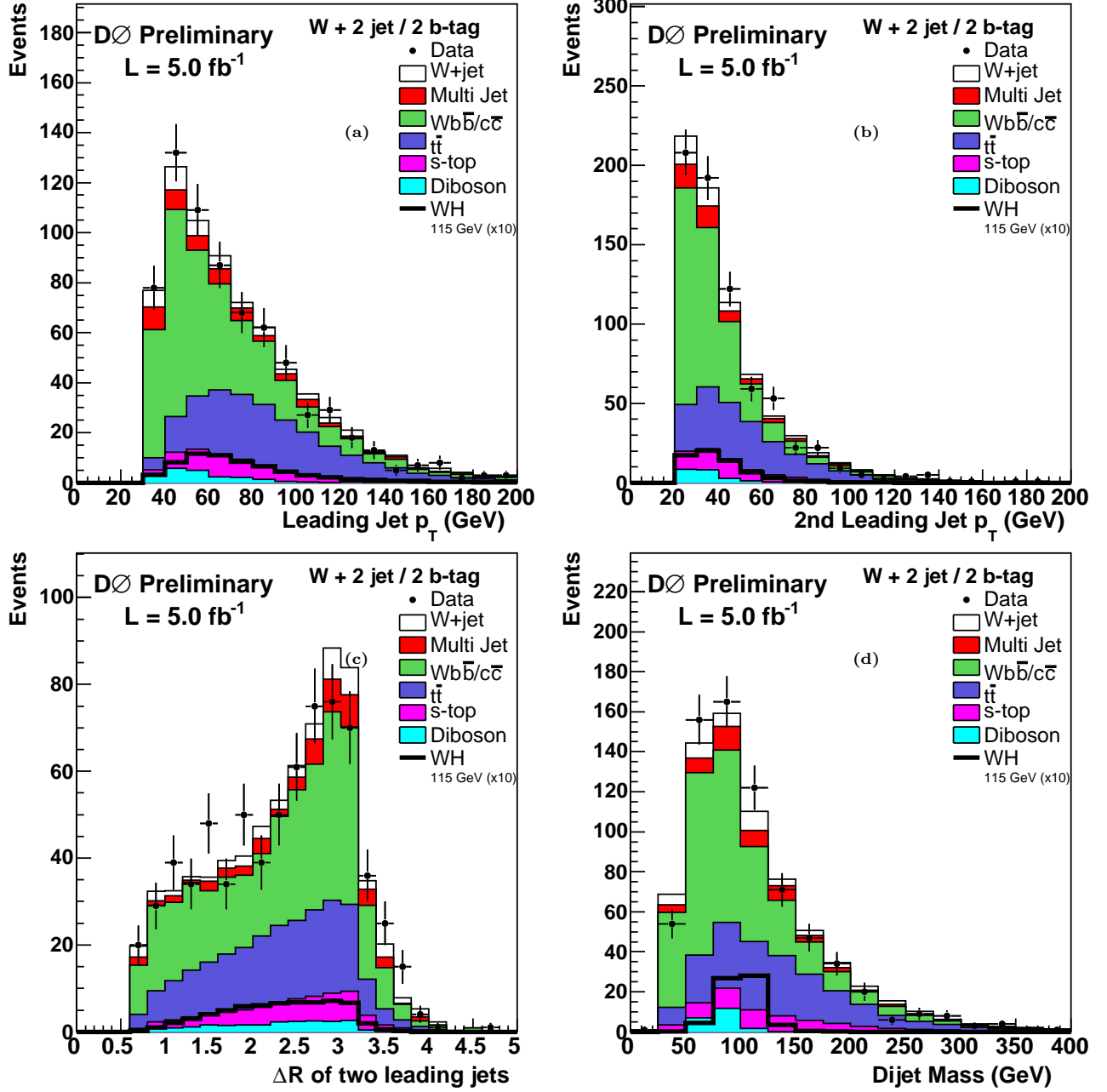


FIG. 4: Distribution in the  $W + 2 \text{ jet}$  sample with two b-tagged jets of the  $p_T$  of (a) the leading and (b) the next to leading jet, (c) the distance in the  $\eta - \phi$  plane between the two jets and (d) the dijet mass between the two jets compared with the simulated expectation. The simulation is normalized to the integrated luminosity of the data sample using the expected cross sections except for the  $W+$  jets sample which is normalized to the data in the untagged sample, taking into account all the other backgrounds. Also shown is the contribution expected for SM  $WH$  production with  $m_H = 115 \text{ GeV}$ , multiplied by a factor 10.

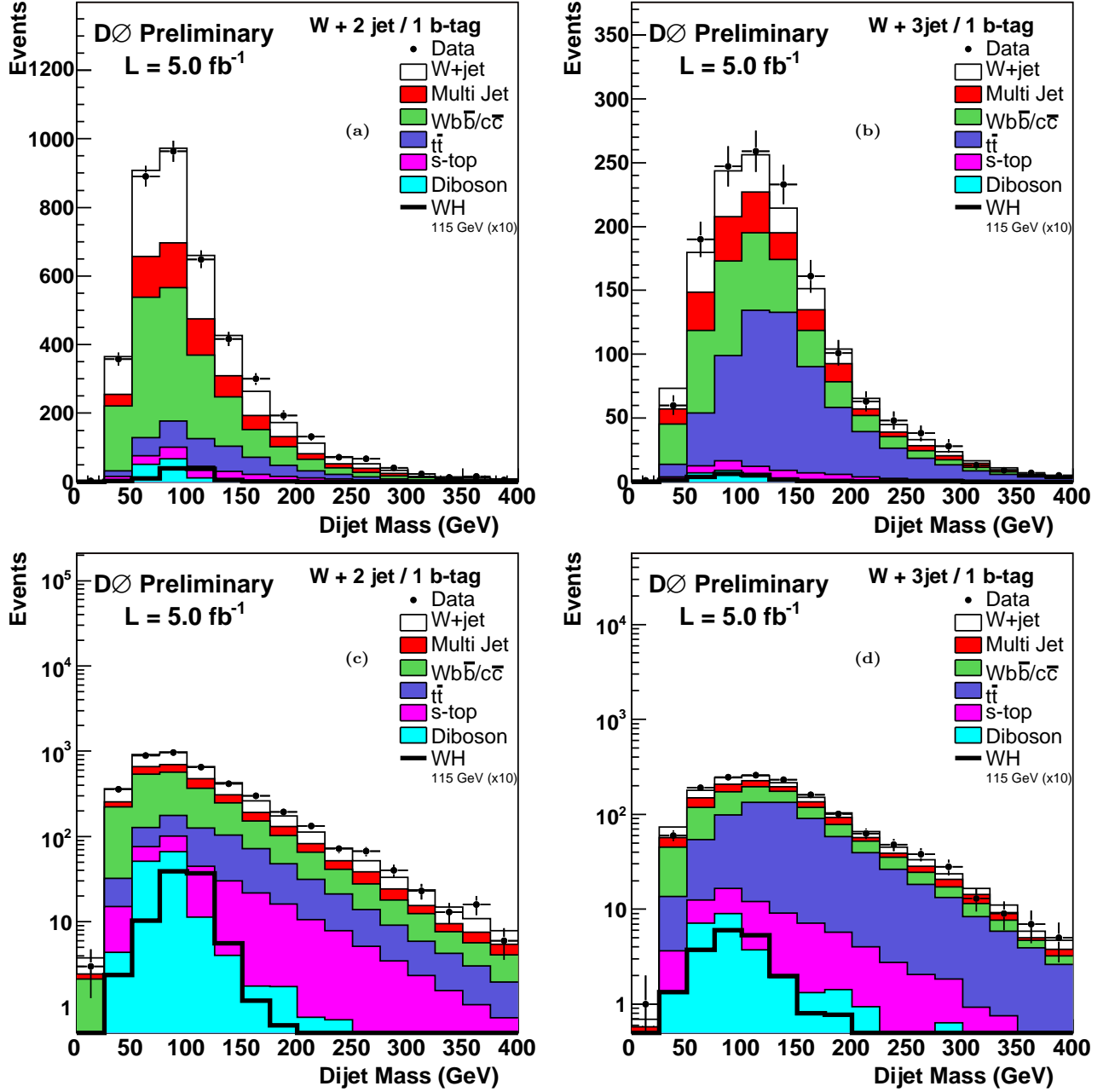


FIG. 5: a) (b) dijet invariant mass in  $W + 2(3)$  jet events when exactly one jet is b-tagged. c) (d) same distributions in Logarithmic scale. The simulated processes are normalized to the integrated luminosity of the data sample using the expected cross sections except for the  $W +$  jets sample which is normalized to the data in the untagged sample, taking into account all the other backgrounds. Also shown is the contribution expected for SM  $WH$  production with  $m_H = 115$  GeV, multiplied by a factor 10.

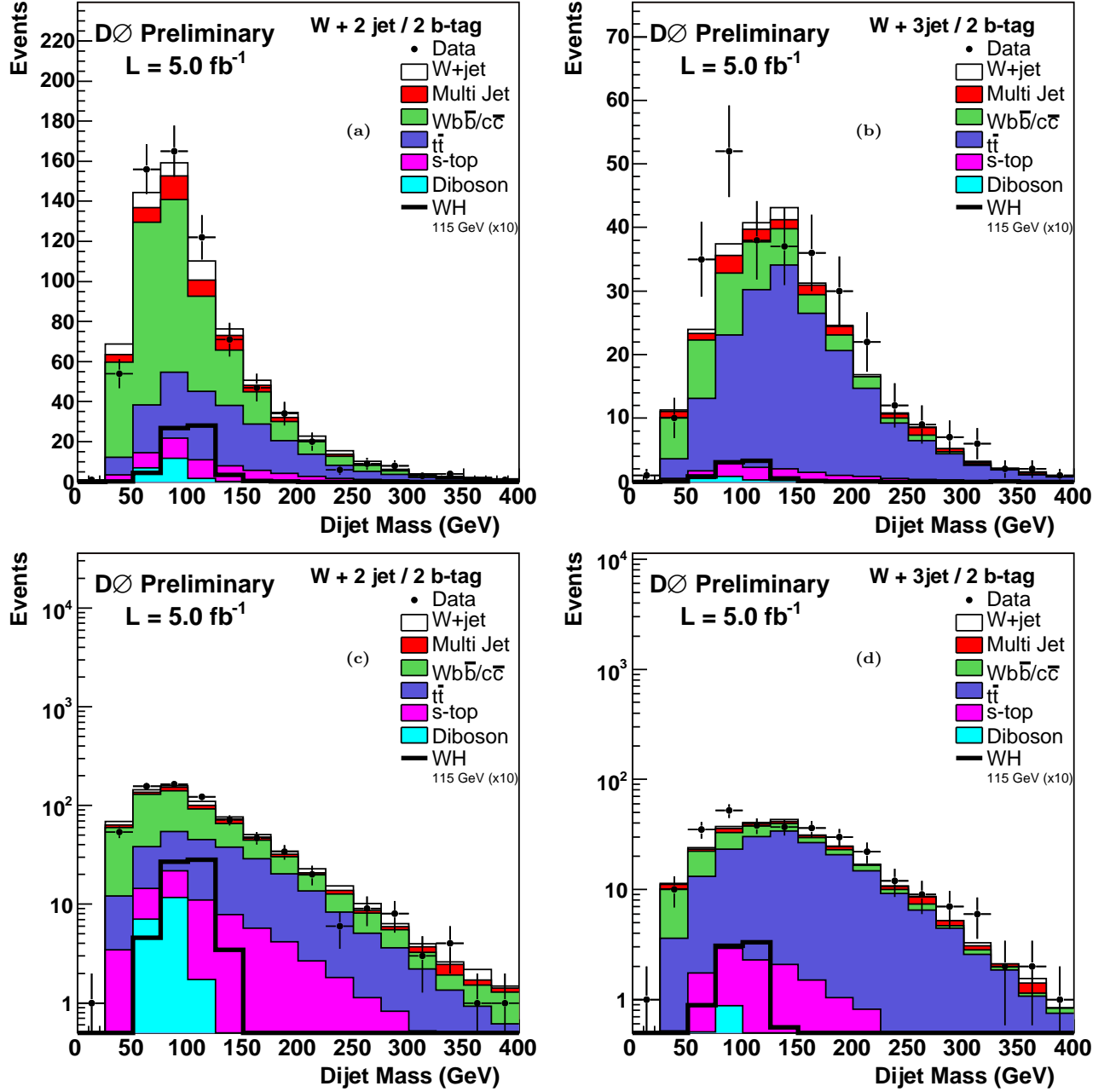


FIG. 6: a) (b) dijet invariant mass in  $W + 2(3)$  jet events when two leading jets are b-tagged. c) (d) same distributions in Logarithmic scale. The simulated processes are normalized to the integrated luminosity of the data sample using the expected cross sections except for the  $W + \text{jets}$  sample which is normalized to the data in the untagged sample, taking into account all the other backgrounds. Also shown is the contribution expected for SM  $WH$  production with  $m_H = 115 \text{ GeV}$ , multiplied by a factor 10.

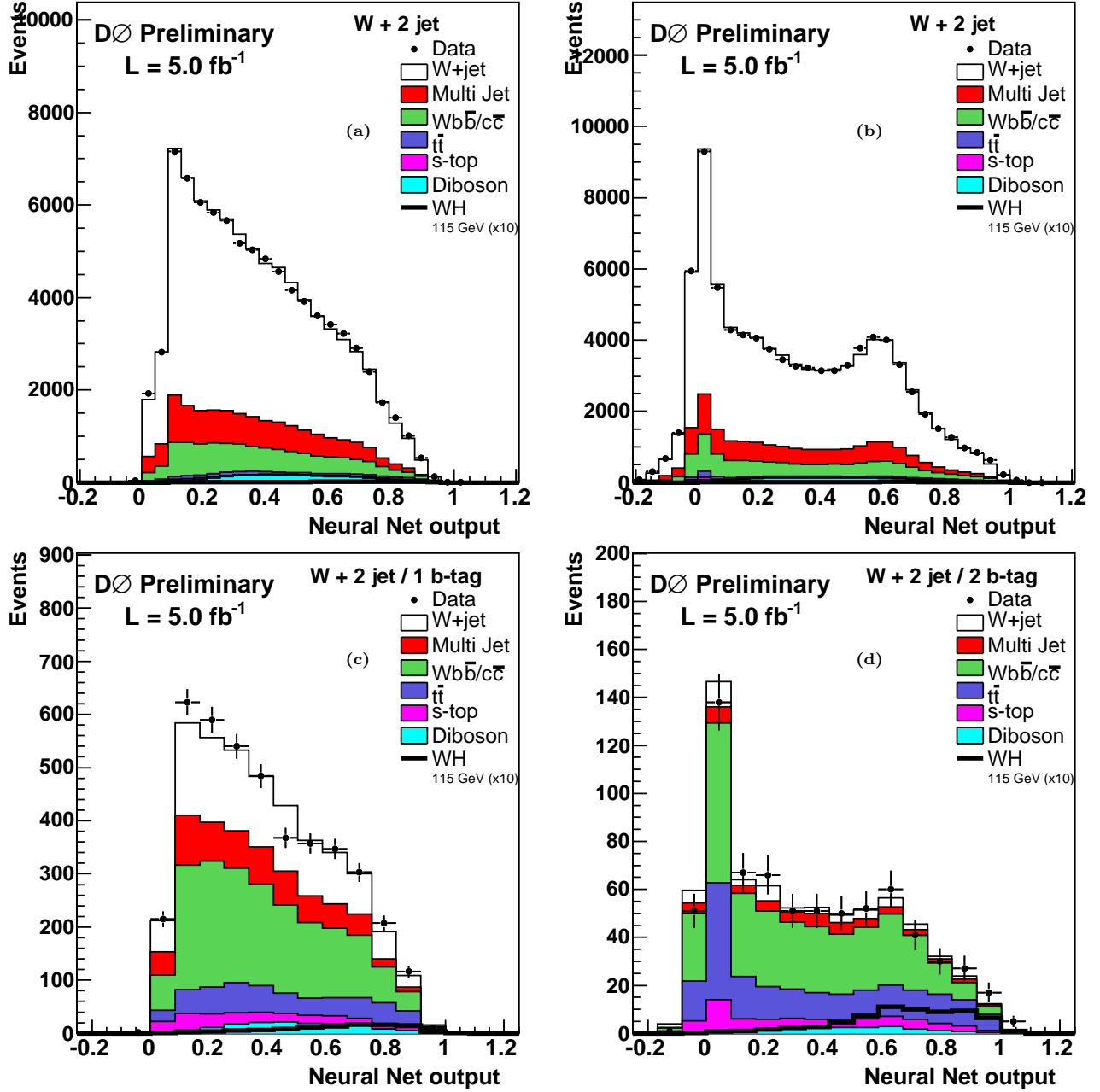


FIG. 7: Distributions (with linear vertical scale) of the neural network output compared with the simulated expectation: a) before  $b$ -tagging for the single-tag NN ; b) before  $b$ -tagging for the double-tag NN ; c) in the single  $b$ -tag sample for the single-tag NN ; d) in the double  $b$ -tag sample for the double-tag NN. The simulation is normalized to the integrated luminosity of the data sample using the expected cross sections except for the  $W + \text{jets}$  sample which is normalized to the data in the untagged sample, taking into account all the other backgrounds. The  $WH$  expected contribution for  $m_H = 115 \text{ GeV}$ , multiplied by a factor 10, is peaking at high values of the NN output as shown in c) and d).

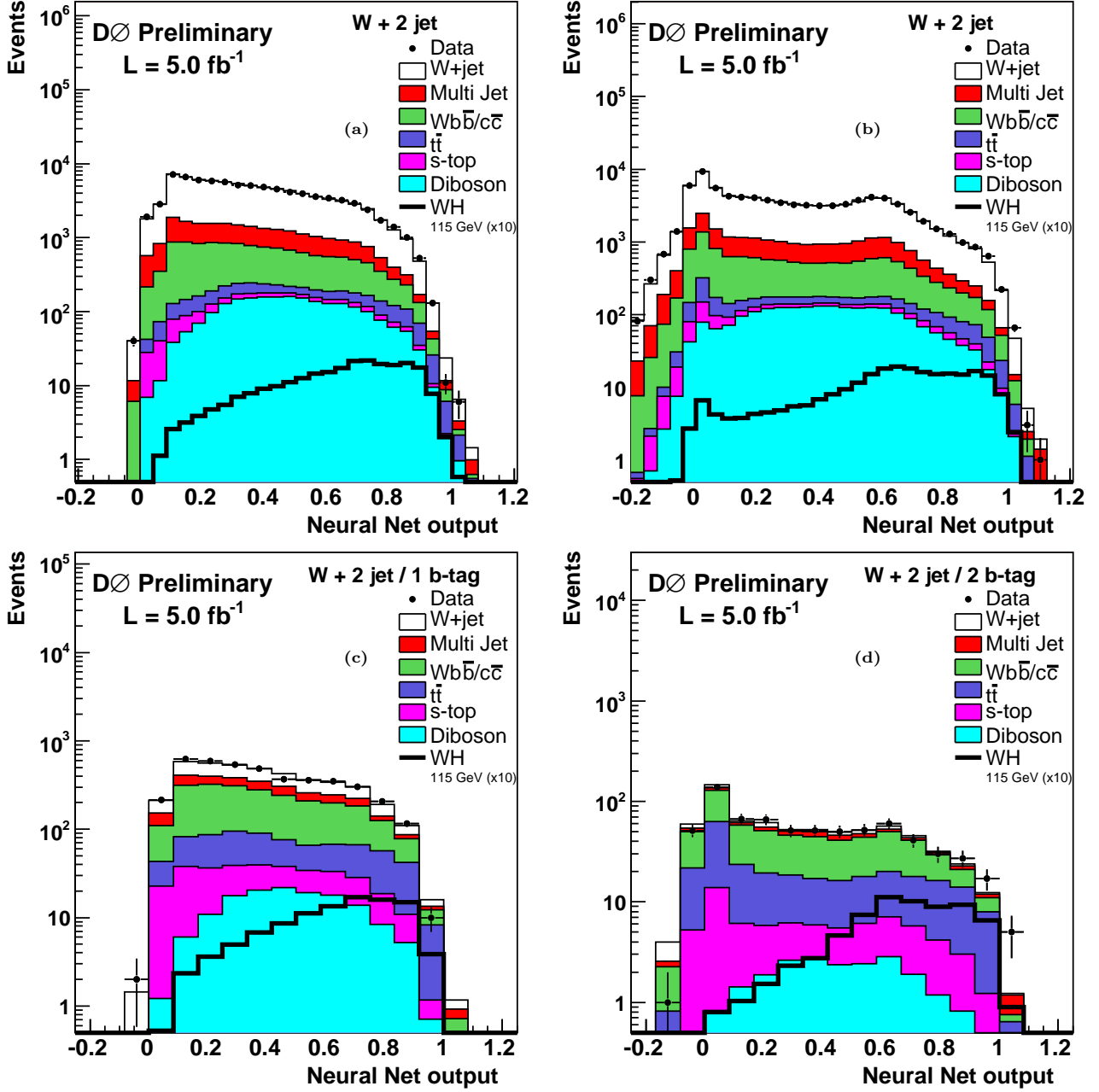


FIG. 8: Distributions (with logarithmic vertical scale) of the neural network output compared with the simulated expectation: a) before b-tagging for the single-tag NN ; b) before b-tagging for the double-tag NN ; c) in the single b-tag sample for the single-tag NN ; d) in the double b-tag sample for the double-tag NN. The simulation is normalized to the integrated luminosity of the data sample using the expected cross sections except for the  $W + \text{jets}$  sample which is normalized to the data in the untagged sample, taking into account all the other backgrounds. The  $WH$  expected contribution for  $m_H = 115 \text{ GeV}$ , multiplied by a factor of 10, is peaking at high values of the NN output as shown in c and d).

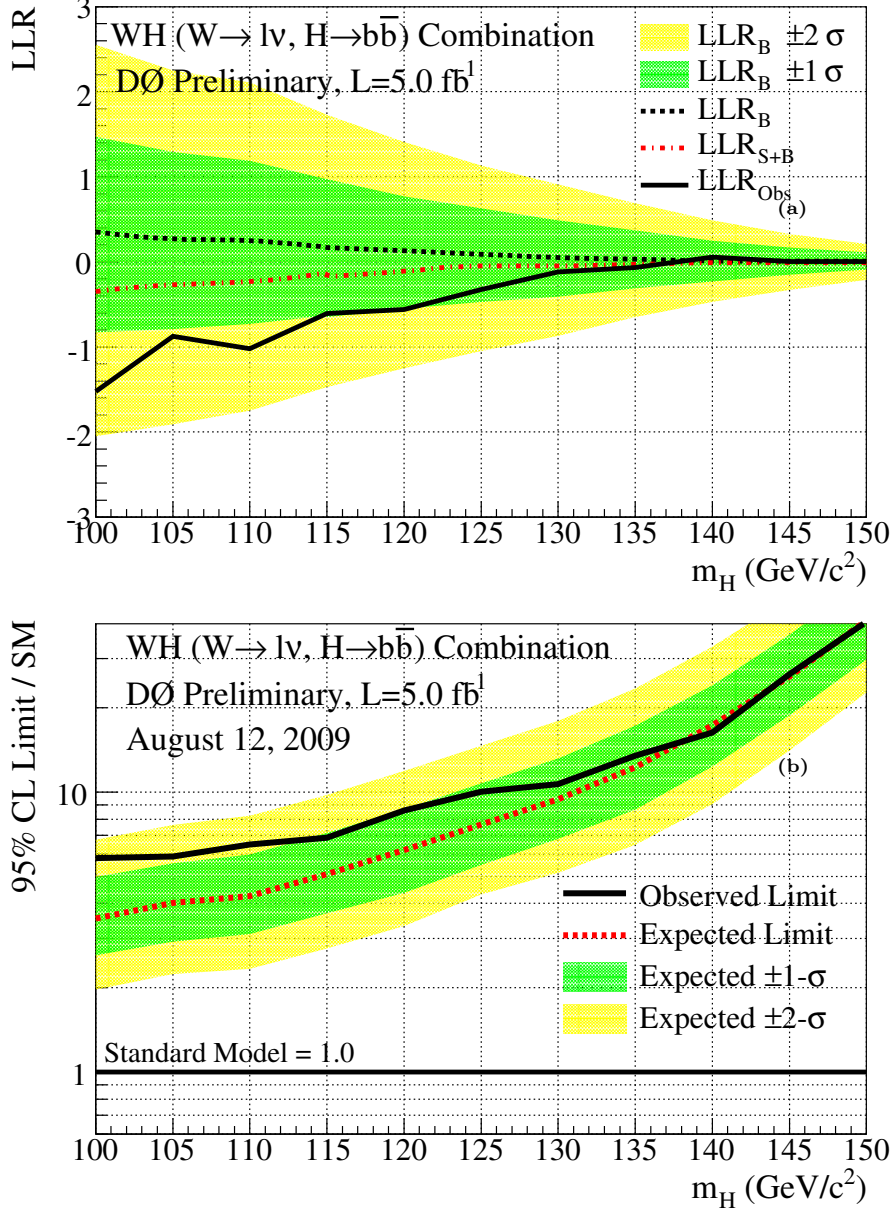


FIG. 9: a) Log-likelihood ratio distribution for the  $WH \rightarrow l\nu b\bar{b}$  2+3 jet channel. The dashed lines represent  $LLR_b$  (upper line)  $LLR_{s+b}$  (lower line), the full line represents  $LLR_{\text{obs}}$ ; for  $LLR_b$ , 1 and 2 standard deviation bands are drawn, cf section 8. b) Expected (median) and observed 95% C.L. upper limits on the cross section ratios for the combined  $WH \rightarrow e, \mu\nu b\bar{b} W + 2 \text{ jet}$  analyses (single- and double-tag, CC electrons + muons) in the  $m_H = 100 - 150 \text{ GeV}$  mass range. The solid line at  $y = 1$  indicates the 95% C.L. exclusion of the SM expectation.